

# A quantum emitter coated with graphene interacting in the strong coupling regime

Mehmet Günay<sup>1,2,\*</sup>, Vasilios Karanikolas<sup>2,3</sup>, Ramazan Sahin<sup>3</sup>,  
 Rasim Volga Ovali<sup>4</sup>, Alpan Bek<sup>5,‡</sup>, and Mehmet Emre Tasgin<sup>2,‡</sup>  
<sup>1</sup>*Department of Nanoscience and Nanotechnology, Faculty of Arts and Science,  
 Mehmet Akif Ersoy University, 15030 Burdur, Turkey*  
<sup>2</sup>*Institute of Nuclear Sciences, Hacettepe University, 06800 Ankara, Turkey*  
<sup>3</sup>*Faculty of Science, Department of Physics, Akdeniz University, 07058 Antalya, Turkey*  
<sup>4</sup>*Department of Materials Science and Nanotechnology Engineering,  
 Recep Tayyip Erdogan University, 53100 Rize, Turkey and*  
<sup>5</sup>*Department of Physics, Middle East Technical University, 06800 Ankara, Turkey*

We demonstrate the strong coupling of a quantum dot and a graphene spherical shell coating it. The simulations are the exact solutions of 3D Maxwell equations. Interaction produces sharp hybrid modes, even when the two are off-resonant, which are voltage-tunable (continuously) in an 80 meV interval. Despite a voltage-tunable quantum dot, the coupling of the light to these "very sharp" plexcitonic resonances is order of magnitude larger than its coupling to a quantum dot. Hence, our results are very attractive for the sensing applications. Moreover, on a simple theoretical model, we explain why such sharp, highly tunable, resonances emerge.

## I. INTRODUCTION

Graphene is a material with superior optical, electronic and mechanical properties [1–5]. And, it can be used for replacing noble metals (mainly Au and Ag) for applications operating at near to far infrared (IR) wavelengths [6]. Graphene possesses an advantage over noble metals because it has smaller material losses [7] and also its optical properties are tunable [8], thus allowing the design of multipurpose applications [9–11].

In recent years, graphene has also been recognized as a promising active material for super-capacitors. Studies show that having large surface area is essential for such applications [12, 13]. In that respect, a spherical geometry (graphene nano-ball) is suggested for increasing the surface area. Then, it was shown that a graphene mesoporous structure with an average pore diameter of 4.27 nm, can be fabricated via chemical vapor deposition technique [14]. Additionally, self-crystallized graphene and graphite nano-balls have been recently demonstrated via Ni vapor-assisted growth [15]. Utilization of such growth techniques or in-liquid synthesis methods [16] can be employed to construct nanoparticle-graphene composite structures which operate at strong-coupling regime. In many of studies on such nanoscale composites, the focus of attention resided mainly on electrical properties. It is also intriguing to study the optical applications of the graphene spherical shell (GSS) structures [17]. In addition, the electromagnetic response of spherical shells has also been studied in terms of their plasmonic responses [18, 19].

Graphene plasmons (GPs) can be tuned continuously by applying a voltage or can be adjusted by electrostatic doping [20] besides trapping the incident light into small volumes [21, 22]. This tuning provides incredible poten-

tial in a vast amount of applications, such as sensing [23], switching [8], and meta-materials [24]. Placing a quantum emitter (QE), such as a quantum dot (QD), in close proximity to a graphene nano-structure can yield strong interaction [21] and modulations in optical properties. Usually the interactions between QE placed in a nano-structured environment are described through investigating the QE's lifetime, calculating the Purcell factor [21]. For such simulations, the QE-nano-structure interaction is described in terms of non-Hermitian of quantum electrodynamics, and the QE is assumed as a point dipole source. Moreover, the interaction between the QE and an infinite graphene layer has been investigated experimentally by measuring the relaxation rate for varying the distance between them [25] and varying the chemical potential value of the graphene layer [26]. The QEs used are erbium ions with a transition energy close to the telecommunication wavelength, where the graphene nano-structures can have a plasmonic response for specific chemical potential values. Moreover, there are variety of molecules and quantum emitters also operating at infrared wavelengths [27, 28].

In this paper, we demonstrate the strong coupling between a 5 nm-radius quantum dot (QD) and a graphene spherical shell, of the same size, coating the QD as shown in Fig. 1. We show that, in this way, the strong coupling between a QD and graphene shell can be achieved even in a single quantum emitter level. Interestingly, the splitting of 80 meV between hybrid modes could be obtained due to the strong coupling even when the spectra of the QD does not overlap with the graphene shell (when the two, actually, are off-resonant to each-other). The continuous tuning not only allows the swap of a spectral region of 80 meV but also provides a hybrid mode of a spectral width very narrow (high-quality, larger lifetime) compared to the graphene's width. The spectral positions of the these hybrid modes can be controlled via tuning the chemical potential of the graphene shell. Beyond demonstrating these effects via exact solutions

\* gunaymehmt@gmail.com

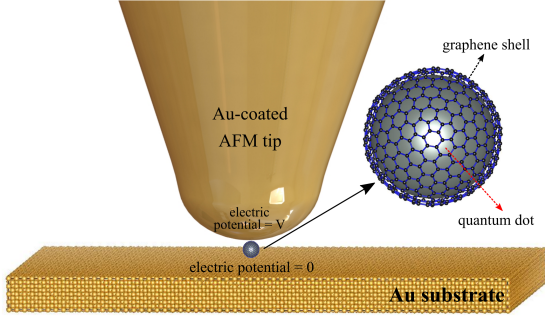


FIG. 1. In the proposed experimental setup, the hybrid structure, a QD coated with GSS, is placed between Au-substrate and Au-coated AFM tip with zero and finite electrical potential respectively.

of the 3D Maxwell equations, i.e., taking the retardation effects into account, we also demonstrate that the same effects are already predicted by a simple analytical model. We explain the physics, i.e., why such a sharp hybrid mode appear simply via the analytical model.

Achieving such 'tunable' thin plasmonic (plexcitonic) modes are invaluable for sensing applications, since one of the hybrid modes has sharper line-width carrying potential for enhanced Figure of Merit (FOM) sensing. We remark that the spectral position of a QD (in general a QE) is also tunable via voltage. The coupling of light to a QD, however, is order of magnitude lower compared to a graphene nano-shell which also provides an intense hot-spot.

The manuscript is organized as follows. We first present the exact solutions of the 3D-Maxwell equations, specifically, the absorption spectrum of the GSS, the semi-conducting sphere individually and the combination of a QE with a GSS (the full case), respectively in Sec. II. Next, we describe the theoretical model and derive an effective Hamiltonian for a two-level system (QE) coupled to GPs in Sec. III where we derive the equations of motion for suggested structure and obtain *a single equation* for the steady-state plasmon amplitude. A summary appears in Sec. IV.

## II. ELECTROMAGNETIC SIMULATIONS OF THE ABSORPTION OF A GRAPHENE COATED SEMI-CONDUCTING SPHERE

When the absorption peak of the QE matches the GP resonance, we observe a splitting in the absorption band due to the interaction between the exciton polariton mode, of the semi-conducting sphere, with the localized surface GP mode, supported by the GSS. To prove this, we perform electromagnetic simulations by using

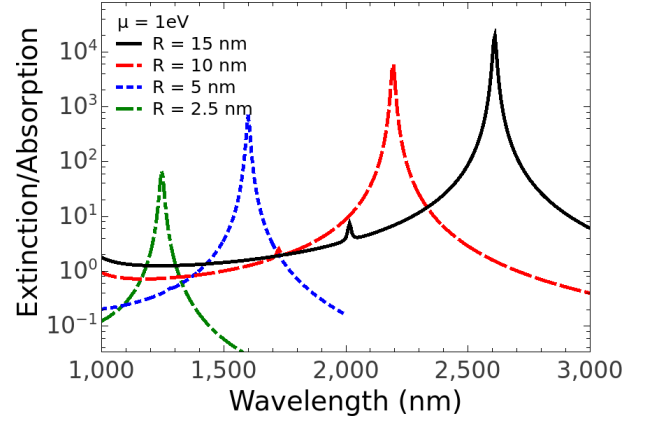


FIG. 2. Absorption spectrum of the GSS, varying the excitation wavelength. We keep fixed the value of the chemical potential,  $\mu = 1$  eV, of the GSS, for different values of its radius,  $R = 2.5$  nm, 5 nm, 10 nm and 15 nm.

MNPBEM package [29], through solving the Maxwell equations in 3-dimensions. This splitting is connected to the energy exchange between the two modes. Due to the large splitting the system enters the strong coupling regime, where a splitting of 80 meV between the hybrid-modes is observed [30]. These type of collective modes have been also named as plexcitons [31]. We stress out that the QE coated with GSS has been experimentally demonstrated [32]. In this section, we start with presenting the mathematical framework and the expressions that give the dielectric permittivity of the GSS and of the semi-conducting QE. Next we present results regarding the absorption spectrum of the GSS, the QE and the full case of QE with a GSS coating.

The optical response of graphene is given by its in-plane surface conductivity,  $\sigma$ , in the random phase approximation [33, 34]. This quantity is mainly determined by electron-hole pair excitations, which can be divided into intraband and interband transitions  $\sigma = \sigma_{\text{intra}} + \sigma_{\text{inter}}$ . It depends on the chemical potential ( $\mu$ ), the temperature ( $T$ ), and the scattering energy ( $E_S$ ) values [35].

The intraband term  $\sigma_{\text{intra}}$  describes a Drude modes response, corrected for scattering by impurities through a term containing  $\tau$ , the relaxation time. The relaxation time,  $\tau$ , causes the plasmons to acquire a finite lifetime and is influenced by several factors, such as collisions with impurities, coupling to optical phonon and finite-size effects. In this paper, we assume that  $T = 300$  K and  $\tau = 1$  ps. In addition, we vary the value of chemical potential [9],  $\mu$ , for active tuning of GPs.

In Fig. 2 and Fig. 3, we present the extinction spectrum of the GSS by a plane wave illumination. In both figures we observe a peak in the extinction spectrum, this peak value is due to the excitation of localized surface plasmon (LSP) mode supported by the GSS. In particular, the LSP resonance frequency is given as a solution of the equation [18]:

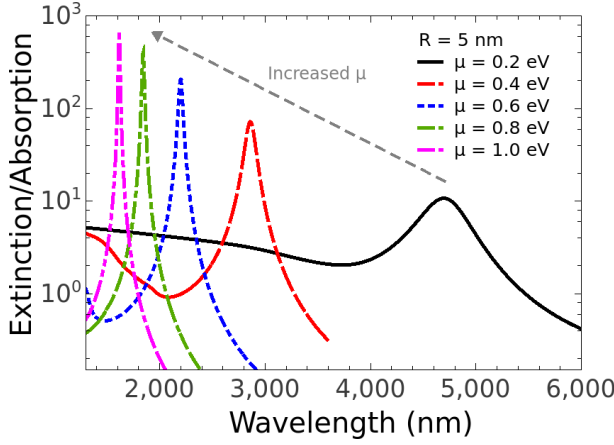


FIG. 3. Extinction/absorption spectrum of the GSS, varying the excitation wavelength. We keep fixed the radius,  $R = 5$  nm, of the GSS, for different values of chemical potential,  $\mu = 0.2$  eV,  $0.4$  eV,  $0.6$  eV,  $0.8$  eV and  $1.0$  eV.

$$\frac{i\epsilon\omega_l}{2\pi\sigma(\omega_l)} = \left(1 + \frac{1}{2l+1}\right) \frac{l}{R}, \quad (1)$$

where  $R$  is the radius of the GSS,  $\epsilon$  is the dielectric permittivity of the surrounding medium and the space inside the GSS and  $l$  is the resonance eigenvalue which is connected with the expansion order. Here, we focus on GSS radii that  $R \ll \lambda$ , where  $\lambda$  is the excitation wavelength, thus we focus on the dipole mode  $l = 1$ . Since,  $R \ll \lambda$ , the extinction and the absorption have essentially the same value (we disregard its scattering). Moreover, the LSP resonance depends on the intraband contributions of the surface conductivity, which, in the limit  $\mu/\hbar\omega \gg 1$ ,  $\sigma(\omega) = 4ia\mu/\hbar\omega$ , ignoring the plasmon lifetime. Then, the LSP resonance wavelength ( $\lambda_1$ ) has the value:

$$\lambda_1 = 2\pi c \sqrt{\frac{\hbar\epsilon}{\pi a\mu} \frac{1}{12}} R. \quad (2)$$

In boundary element simulations, using MNPBEM [29], the GSS is modeled as a thin layer of thickness  $d = 0.5$  nm, with a dielectric permittivity [36], ( $\epsilon(\omega)$ )

$$\epsilon(\omega) = 1 + \frac{4\pi\sigma(\omega)}{\omega d}, \quad (3)$$

where the surface conductivity is given by Eq. 1 [9].

In Fig. 2, we present the absorption spectrum of the GSS in near IR region, considering different values of its radius  $R = 2.5$  nm,  $5$  nm,  $10$  nm and  $15$  nm. We consider a fixed value for the chemical potential,  $\mu = 1$  eV and observe that by increasing the radius of the GSS the surface plasmon resonance is red-shifted as is predicted by Eq. 2. The dipole surface plasmon resonance from Fig. 2 for  $R = 10$  nm is  $2190$  nm and from numerically solving

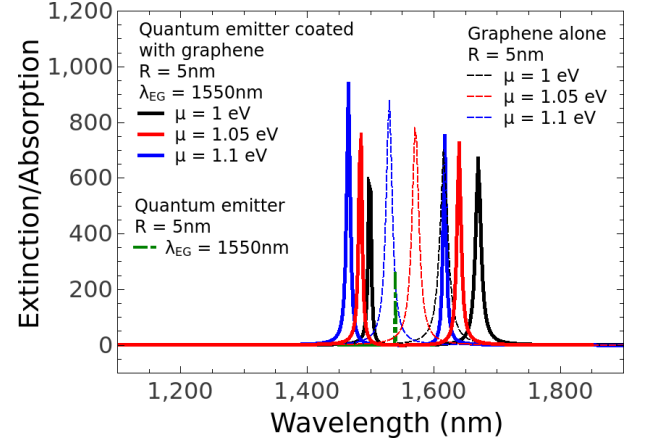


FIG. 4. Absorption spectra of the QE coated with the GSS with respect to excitation wavelength. Different values of the chemical potential are employed while the QE transition energy is kept constant at  $\lambda_{eg} = 1550$  nm. More details on simulation parameters are given in the inset.

Eq. 1 it is  $2120$  nm, validating our approach. Moreover, increasing the GSS radius the absorption strength gets higher.

In Fig. 3, we present the extinction spectrum of the GSS, for fixed radius  $R = 5$  nm, for different values of the chemical potential,  $\mu = 0.2$  eV,  $0.4$  eV,  $0.6$  eV,  $0.8$  eV and  $1.0$  eV. As the value of the chemical potential increases the GP resonance is shifted to lower wavelengths as expected from Eq. 2. The physical explanation for such behavior is that the optical gap increases as the chemical potential value increases, thus the surface plasmon resonance blue-shifts. For exploring the effect of coupling, we placed a QD (QE) inside GSS. The optical properties of the QE are also described through its absorption spectrum. We here stress out that we do not take into account the emission of the QE itself. Response of a QD or QE can be safely modeled by a Lorentzian dielectric function [37, 38].

$$\epsilon_{eg}(\omega) = \epsilon_{\infty} - f \frac{\omega_{eg}^2}{\omega^2 - \omega_{eg}^2 + i\gamma_{eg}\omega}, \quad (4)$$

where  $\epsilon_{\infty}$  is the bulk dielectric permittivity at high frequencies,  $f$  is the oscillator strength [39, 40] and  $\gamma_{eg}$  is the transition line-width, which is connected to quality of the QE.  $\omega_{eg}$  is connected with the energy from the excited to the ground state of the QE. As the sphere is composed by a semi-conducting material, it supports localized exciton polariton modes. The sphere sizes considered in this paper are much smaller than the excitation wavelength and only the dipole exciton resonance is excited. In the electrostatic limit, condition for exciting the dipole localized exciton resonance is given by the  $Re(\epsilon_{eg}(\omega)) = -2\epsilon$ , where  $\epsilon$  is the dielectric permittivity of the surrounding medium, in this paper we consider  $\epsilon = 1$ . From this resonance condition it becomes apparent that changing the

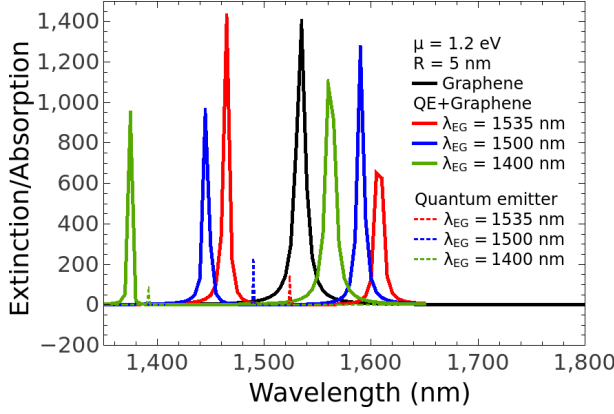


FIG. 5. Absorption spectra of the QE coated with the GSS with respect to excitation wavelength. Fixed value for the chemical potential is taken as  $\mu = 1.2$  eV, while different values of the transition energy of the QE are considered. More details in the inset.

radius of the semi-conducting sphere does not influence its resonance wavelength, as long as  $R \ll \lambda$ . On the other hand, as the level spacing of the QE changes, the position of the dipole localized exciton resonance shifts accordingly.

In Fig. 4, we consider the full case in which the QE is coated by GSS. We simulate the absorption of the combined system in the same spectral region. We start in Fig. 4 by considering the effect of the value of the chemical potential,  $\mu$ , in the absorption of the combined system, where the value of the transition energy of the QE is fixed at  $\lambda_{eg} = 1550$  nm. For the chemical potential  $\mu = 1$  eV the splitting in the absorption spectrum is  $\hbar\Omega = 84$  meV, where we can apparently see that the localized exciton mode is off-resonant to the surface plasmon mode. This means that the interaction between GP and exciton modes is still in the strong coupling regime. In addition, the initial splitting blue-shifts as the value of the chemical potential  $\mu$  increases.

In Fig. 5, we present the absorption of the QE coated with GSS, for  $\mu = 1.2$  eV and the radius of the sphere is  $R = 5$  nm. We consider different values of the transition energy of the QE,  $\lambda_{eg}$ . We observe that by increasing the value of  $\lambda_{eg}$  the resonance of the exciton polariton mode redshifts, similarly the splitting in the extinction/absorption of the combined QE core-GSS nanosystem also redshifts. Initially for  $\lambda_{eg} = 1400$  nm, even the exciton polariton and the GP modes are highly off-resonant, we still observe the plexitonic modes, which can also be read as the existence of the strong coupling between the nanostructures. In the following section, we explain this in more detail with a simple analytical model.

### III. THE ANALYTICAL MODEL

Here, we write the effective Hamiltonian for the GPs coupled to a QE and derive the equations of motion. We consider the QE as a two level system [37] with level

spacing  $\omega_{eg} = 2\pi c/\lambda_{eg}$ . In the steady state, we obtain a single equation. We show that by using this equation one can have a better understanding on the parameters of the combined system.

We consider the dynamics of the total system as follows. The incident light ( $\varepsilon_L$ ) with optical frequency  $\omega = 2\pi c/\lambda$  excites a GP ( $\hat{a}_{GP}$ ), which is coupled to a QE. The Hamiltonian of the system can be written as the sum of the energy of the QE and GP ( $\omega_{GP} = 2\pi c/\lambda_{GP}$ ) oscillations ( $\hat{H}_0$ ) and the energy transferred by the pump source ( $\hat{H}_L$ )

$$\hat{H}_0 = \hbar\omega_{GP}\hat{a}_{GP}^\dagger\hat{a}_{GP} + \hbar\omega_{eg}|e\rangle\langle e| \quad (5)$$

$$\hat{H}_L = i\hbar(\varepsilon_L\hat{a}_{GP}^\dagger e^{-i\omega t} - h.c) \quad (6)$$

and the interaction of the QE with the GP modes ( $\hat{H}_{int}$ )

$$\hat{H}_{int} = \hbar\{\Omega_R^*\hat{a}_{GP}^\dagger|g\rangle\langle e| + \Omega_R|e\rangle\langle g|\hat{a}_{GP}\}, \quad (7)$$

where the parameter  $\Omega_R$ , in units of frequency, is the coupling strength between GP and the QE.  $|g\rangle$  ( $|e\rangle$ ) is the ground (excited) state of the QE. In the strong coupling limit, one needs to consider counter-rotating terms in the interaction Hamiltonian [41], but there is still no analytically exact solution [42]. Instead of pursuing a full consideration, left for future work, we demonstrate here RWA, giving consistent results for the structure considered in this work. Moreover, we are interested in intensities but not in the correlations, so we replace the operators  $\hat{a}_i$  and  $\hat{\rho}_{ij} = |i\rangle\langle j|$  with complex number  $\alpha_i$  and  $\rho_{ij}$  [43] respectively and the equations of motion can be obtained as

$$\dot{\alpha}_{GP} = -(i\omega_{GP} + \gamma_{GP})\alpha_{GP} - i\Omega_R^*\rho_{ge} + \varepsilon_L e^{-i\omega t}, \quad (8a)$$

$$\dot{\rho}_{ge} = -(i\omega_{eg} + \gamma_{eg})\rho_{ge} + i\Omega_R\alpha_{GP}(\rho_{ee} - \rho_{gg}), \quad (8b)$$

$$\dot{\rho}_{ee} = -\gamma_{ee}\rho_{ee} + i\{\Omega_R^*\alpha_{GP}\rho_{ge} - c.c\}, \quad (8c)$$

where  $\gamma_{GP}$  and  $\gamma_{eg}$  are the damping rates of the GP mode and of the off-diagonal density matrix elements of the QE, respectively. The values of the damping rates are considered as the same with previous section. The conservation of probability  $\rho_{ee} + \rho_{gg} = 1$  with the diagonal decay rate of the QE  $\gamma_{ee} = 2\gamma_{eg}$  accompanies Eqs.(8a-8c). In the steady state, one can define the amplitudes as

$$\alpha_{GP}(t) = \tilde{\alpha}_{GP}e^{-i\omega t}, \quad \rho_{ge}(t) = \tilde{\rho}_{ge}e^{-i\omega t}, \quad (9)$$

where  $\tilde{\alpha}_{GP}$  and  $\tilde{\rho}_{ge}$  are constant in time. By inserting Eq.(9) into Eqs.(8a-8c), the steady-state solution for the GP mode can be obtained as

$$\tilde{\alpha}_{GP} = \frac{\varepsilon_L[i(\omega_{eg} - \omega) + \gamma_{eg}]}{(\omega - \Omega_+)(\omega - \Omega_-) + i\Gamma(\omega)}, \quad (10)$$

where  $\Omega_{\pm} = \delta_{\pm} \pm \sqrt{\delta_{\pm}^2 - |\Omega_R|^2 y + \gamma_{eg}\gamma_{GP}}$  defines hybrid mode resonances [44] and  $\Gamma(\omega) = [\gamma_{eg}(\omega_{GP} - \omega) + \gamma_{GP}(\omega_{eg} - \omega)]$  with  $\delta_{\pm} = (\omega_{GP} \pm \omega_{eg})/2$  and population inversion  $y = \rho_{ee} - \rho_{gg}$  terms.

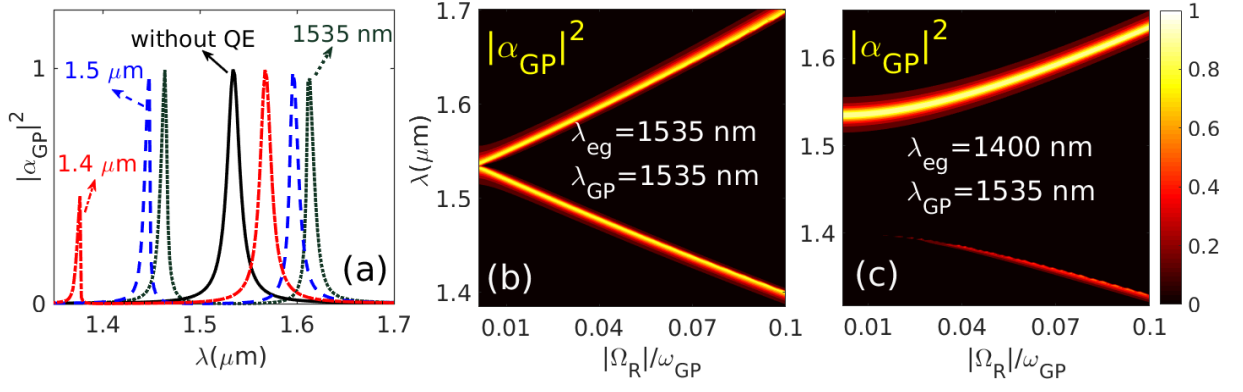


FIG. 6. The scaled absorption intensity of the GP ( $|\alpha_{GP}|^2$ ) as a function of excitation wavelength  $\lambda$ , obtained from Eq. (8a-8c). (a) In the absence (black-solid) and in the presence of the QE having resonance at  $\lambda_{eg} = 1535$  nm (dark gray-dotted),  $\lambda_{eg} = 1500$  nm (blue-dashed) and  $\lambda_{eg} = 1400$  nm (red-dashed-dotted) for a fixed coupling strength,  $\Omega_R = 0.05 \omega_{GP}$ . Variation of the resonance intensity of GP with excitation wavelength  $\lambda$  and coupling strength  $\Omega_R$  for (b)  $\lambda_{eg} = 1535$  nm and (c)  $\lambda_{eg} = 1400$  nm. Here we use  $\gamma_{GP} = 0.005 \omega_{GP}$  and  $\gamma_{eg} = 10^{-5} \omega_{GP}$ .

It is important to note that the results presented in Fig. 6 and Fig. 7 are the exact solutions of Eqs.(8a-8c). We study the steady-state in Eq.(10) to gain a better understanding over the parameters and avoid time consuming electromagnetic 3D simulations of the combined system. Moreover, we hereafter calculate the intensity of the GP mode in Eq. (8a), which is related to the absorption from the nanostructure [32], to compare the results with the electromagnetic 3D-simulations.

To find the modulation of the intensities of the hybrid modes in the presence of QE, we use different resonance values of the QE,  $\lambda_{eg} = 2\pi c/\omega_{eg} = 1535$  nm 1500 nm 1400 nm in Fig. 6a. The quantitative results comparing with the numerical simulations in Fig. 5, which takes retardation effects into account, are obtained. We also show the evolution of the hybrid-modes by varying interaction strength  $|\Omega_R|$  for zero detuning ( $\delta_- = 0$ ) in Fig. 6b, and for highly off-resonant case in Fig. 6c. The strong coupling regime is reached if  $\Omega_R^2 > (\gamma_{GP}^2 + \gamma_{eg}^2)/2$  [45], that is the coupling strength exceeds the sum of the dephasing rates. When QE and GP are resonant [see Fig. 6b] a dip starts to appear around  $|\Omega_R| \approx \gamma_{GP}$ . This can be also read from Eq. (10). That is when  $\omega_{eg} = \omega_{GP} = \omega$ , the Eq. (10) becomes  $\tilde{\alpha}_{GP} \propto \gamma_{eg}/(|\Omega_R|^2 y + \gamma_{GP} \gamma_{eg})$ . Since  $\gamma_{eg}$  is very small from other frequencies, with increasing  $|\Omega_R|$ ,  $\tilde{\alpha}_{GP}$  becomes smaller compared to case obtained without QE. Beyond a point, where the transparency window appears [37], there emerge two different peaks centered at frequencies  $\Omega_{\pm}$ . And, the separation becomes larger as the  $\Omega_R$  increases.

This argument is not valid when GP and level spacing of the QE are highly off-resonant. In this case, to make second peak significant, the interaction strength has to be much larger than  $\gamma_{GP}$  [see Fig. 6c]. The dip can be seen at  $\omega_{eg}$ , which is out of the GP resonance window and it may not be useful for practical applications. However, having sharp peak, due to strong coupling between off-resonant

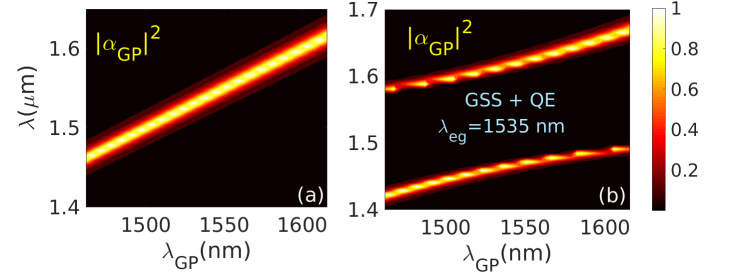


FIG. 7. The scaled field intensity of the GP ( $|\alpha_{GP}|^2$ ) as a function of excitation wavelength  $\lambda$  and GP resonance  $\lambda_{GP}$ , when the GSS is alone (a) and with QE (b). We scale GP intensity with its maximum value and the parameters are used as:  $\Omega_R = 0.1 \omega_{eg}$ ,  $\gamma_{GP} = 0.01 \omega_{eg}$  and  $\gamma_{eg} = 10^{-5} \omega_{eg}$ .

particles, can be very useful for the sensing applications. The reason for that it has smaller line-width and can be tuned by changing chemical potential. To show this, in Fig. 7, we plot the evolution of the field intensity of the GP ( $|\alpha_{GP}|^2$ ) as a function of excitation wavelength  $\lambda$  and GP resonance  $\lambda_{GP}$ , when graphene is alone Fig. 7a and with QE Fig. 7b. It can be seen from Fig. 7b that it is possible to control the positions and line-widths of the hybrid resonances by adjusting  $\mu$ . The similar behavior is also obtained in MNPBEM simulation [see Fig. 4].

#### IV. SUMMARY

In summary, we investigate the optical response of the GPs for the spherical shell geometry in the presence and absence of the QE. We show that there is a tunability of the optical response of the GSS through changing the value of the chemical potential and its radius. For the combined system (the QE covered with a graphene layer) we observe a splitting in the absorption band. This is due to the strong coupling regime where splitting of up



to 80 meV are observed in a single QE limit. We also discuss the case when the QE and GP are off-resonant, and observe that the system can hold strong coupling. The results of the theoretical model, we present here, support the exact solutions of the 3D-Maxwell equations obtained from MNPBEM simulations.

Our results can contribute to controlling light-matter interactions at the nanometer scale and find potential from all-optical switch nonlinear devices to sensing applications with current experimental ability for fabrica-

tion. Extreme field confinement, device tunability and low losses make such structures even more attractive in the future studies.

## ACKNOWLEDGMENTS

<sup>‡</sup> Contributed equally. This research was supported by The Scientific and Technological Research Council of Turkey (TUBITAK) Grant No. 117F118.

- 
- [1] Andre K Geim and Konstantin S Novoselov, “The rise of graphene,” in *Nanoscience and Technology: A Collection of Reviews from Nature Journals* (World Scientific, 2010) pp. 11–19.
  - [2] Jianing Chen, Michela Badioli, Pablo Alonso-González, Sukosin Thongrattanasiri, Florian Huth, Johann Osmond, Marko Spasenović, Alba Centeno, Amaia Pesquera, Philippe Godignon, *et al.*, “Optical nano-imaging of gate-tunable graphene plasmons,” *Nature* **487**, 77 (2012).
  - [3] Zhe Fei, AS Rodin, GO Andreev, W Bao, AS McLeod, M Wagner, LM Zhang, Z Zhao, M Thieme, G Dominguez, *et al.*, “Gate-tuning of graphene plasmons revealed by infrared nano-imaging,” *Nature* **487**, 82 (2012).
  - [4] Zheyu Fang, Sukosin Thongrattanasiri, Andrea Schlather, Zheng Liu, Lulu Ma, Yumin Wang, Pulickel M Ajayan, Peter Nordlander, Naomi J Halas, and F Javier García de Abajo, “Gated tunability and hybridization of localized plasmons in nanostructured graphene,” *ACS nano* **7**, 2388–2395 (2013).
  - [5] M Gullans, DE Chang, FHL Koppens, FJ García de Abajo, and Mikhail D Lukin, “Single-photon nonlinear optics with graphene plasmons,” *Physical review letters* **111**, 247401 (2013).
  - [6] F. Javier García de Abajo, “Graphene Plasmonics: Challenges and Opportunities,” *ACS Photonics* **1**, 135–152 (2014), arXiv:1402.1969.
  - [7] Jacob B. Khurgin and Greg Sun, “Impact of surface collisions on enhancement and quenching of the luminescence near the metal nanoparticles,” *Optics Express* **23**, 30739 (2015).
  - [8] Long Ju, Baisong Geng, Jason Horng, Caglar Girit, Michael Martin, Zhao Hao, Hans A Bechtel, Xiaogan Liang, Alex Zettl, Y Ron Shen, *et al.*, “Graphene plasmonics for tunable terahertz metamaterials,” *Nature nanotechnology* **6**, 630 (2011).
  - [9] K S Novoselov, “Electric Field Effect in Atomically Thin Carbon Films,” *Science* **306**, 666–669 (2004).
  - [10] A N Grigorenko, M Polini, and K S Novoselov, “Graphene plasmonics,” *Nat. Photon.* **6**, 749–758 (2012).
  - [11] Tony Low and Phaedon Avouris, “Graphene plasmonics for terahertz to mid-infrared applications,” *ACS Nano* **8**, 1086–101 (2014).
  - [12] Chenguang Liu, Zhenning Yu, David Neff, Aruna Zhamu, and Bor Z Jang, “Graphene-based supercapacitor with an ultrahigh energy density,” *Nano letters* **10**, 4863–4868 (2010).
  - [13] Meryl D Stoller, Sungjin Park, Yanwu Zhu, Jinho An, and Rodney S Ruoff, “Graphene-based ultracapacitors,” *Nano letters* **8**, 3498–3502 (2008).
  - [14] Jung-Soo Lee, Sun-I Kim, Jong-Chul Yoon, and Ji-Hyun Jang, “Chemical vapor deposition of mesoporous graphene nanoballs for supercapacitor,” *ACS nano* **7**, 6047–6055 (2013).
  - [15] Wen-Chun Yen, Yu-Ze Chen, Chao-Hui Yeh, Jr-Hau He, Po-Wen Chiu, and Yu-Lun Chueh, “Direct growth of self-crystallized graphene and graphite nanoballs with ni vapor-assisted growth: From controllable growth to material characterization,” *Scientific reports* **4**, 4739 (2014).
  - [16] Haibo Tan, Jing Tang, Joel Henzie, Yunqi Li, Xingtao Xu, Tao Chen, Zhongli Wang, Jiayu Wang, Yusuke Ide, Yoshio Bando, *et al.*, “Assembly of hollow carbon nanospheres on graphene nanosheets and creation of iron–nitrogen-doped porous carbon for oxygen reduction,” *Acs Nano* **12**, 5674–5683 (2018).
  - [17] Nader Daneshfar and Zeinab Noormohamadi, “Optical surface second harmonic generation from plasmonic graphene-coated nanoshells: influence of shape, size, dielectric core and embedding medium,” *Applied Physics A* **126**, 55 (2019).
  - [18] Thomas Christensen, Antti-Pekka Jauho, Martijn Wubs, and N. Asger Mortensen, “Localized plasmons in graphene-coated nanospheres,” *Physical Review B* **91**, 125414 (2015).
  - [19] Tingting Bian, Railing Chang, and PT Leung, “Optical interactions with a charged metallic nanoshell,” *JOSA B* **33**, 17–26 (2016).
  - [20] Hong-Son Chu and Choon How Gan, “Active plasmonic switching at mid-infrared wavelengths with graphene ribbon arrays,” *Applied Physics Letters* **102**, 231107 (2013).
  - [21] Frank H L Koppens, Darrick E Chang, and F Javier García de Abajo, “Graphene plasmonics: a platform for strong light-matter interactions,” *Nano Lett.* **11**, 3370–7 (2011).
  - [22] Giuseppe Toscano, Søren Raza, Wei Yan, Claus Jepsen, Sanshui Xiao, Martijn Wubs, Antti-Pekka Jauho, Sergey I Bozhevolnyi, and N Asger Mortensen, “Nonlocal response in plasmonic waveguiding with extreme light confinement,” *Nanophotonics* **2**, 161–166 (2013).
  - [23] Yilei Li, Hugen Yan, Damon B Farmer, Xiang Meng, Wenjuan Zhu, Richard M Osgood, Tony F Heinz, and Phaedon Avouris, “Graphene plasmon enhanced vibrational sensing of surface-adsorbed layers,” *Nano letters* **14**, 1573–1577 (2014).

- [24] Osman Balci, Nurbek Kakenov, Ertugrul Karademir, Sinan Balci, Semih Cakmakyapan, Emre O Polat, Humeyra Caglayan, Ekmel Özbay, and Coskun Kocabas, “Electrically switchable metadevices via graphene,” *Science advances* **4**, eaao1749 (2018).
- [25] L Gaudreau, K J Tielrooij, G E D K Prawiroatmodjo, J Osmond, F. J. García de Abajo, and F H L Koppens, “Universal Distance-Scaling of Nonradiative Energy Transfer to Graphene,” *Nano Lett.* **13**, 2030–2035 (2013).
- [26] K. J. Tielrooij, L. Orona, A. Ferrier, M. Badioli, G. Navickaite, S. Coop, S. Nanot, B. Kalinic, T. Cesca, L. Gaudreau, Q. Ma, A. Centeno, A. Pesquera, A. Zurutuza, H. de Riedmatten, P. Goldner, F. J. García de Abajo, P. Jarillo-Herrero, and F. H. L. Koppens, “Electrical control of optical emitter relaxation pathways enabled by graphene,” *Nat. Phys.* **11**, 281–287 (2015).
- [27] Joseph a. Treadway, Geoffrey F. Strouse, Ronald R. Ruminski, and Thomas J. Meyer, “Long-Lived Near-Infrared MLCT Emitters,” *Inorganic Chemistry* **40**, 4508–4509 (2001).
- [28] Jeffrey M Pietryga, Richard D Schaller, Donald Werder, Michael H Stewart, Victor I Klimov, and Jennifer A Hollingsworth, “Pushing the band gap envelope: mid-infrared emitting colloidal PbSe quantum dots.” *J. Am. Chem. Soc.* **126**, 11752–3 (2004).
- [29] Ulrich Hohenester and Andreas Trügler, “Mnpbem—a matlab toolbox for the simulation of plasmonic nanoparticles,” *Computer Physics Communications* **183**, 370–381 (2012).
- [30] Denis G. Baranov, Martin Wersäll, Jorge Cuadra, Tomasz J. Antosiewicz, and Timur Shegai, “Novel Nanostructures and Materials for Strong Light-Matter Interactions,” *ACS Photonics* **5**, 24–42 (2018).
- [31] a Manjavacas, F J García de Abajo, and P Nordlander, “Quantum plexcitonics: strongly interacting plasmons and excitons.” *Nano letters* **11**, 2318–23 (2011).
- [32] Longfei Wu, Hongbin Feng, Mengjia Liu, Kaixiang Zhang, and Jinghong Li, “Graphene-based hollow spheres as efficient electrocatalysts for oxygen reduction,” *Nanoscale* **5**, 10839 (2013).
- [33] Marinko Jablan, Hrvoje Buljan, and Marin Soljačić, “Plasmonics in graphene at infrared frequencies,” *Phys. Rev. B* **80**, 245435 (2009).
- [34] L A Falkovsky, “Optical properties of graphene,” *J. Phys.: Conf. Ser.* **129**, 012004 (2008).
- [35] B Wunsch, T Stauber, F Sols, and F Guinea, “Dynamical polarization of graphene at finite doping,” *New J. Phys.* **8**, 318–318 (2006).
- [36] Ashkan Vakil and Nader Engheta, “Transformation Optics Using Graphene,” *Science* **332**, 1291–1294 (2011), arXiv:1101.3585.
- [37] Xiaohua Wu, Stephen K Gray, and Matthew Pelton, “Quantum-dot-induced transparency in a nanoscale plasmonic resonator,” *Optics express* **18**, 23633–23645 (2010).
- [38] Selen Postaci, Bilge Can Yildiz, Alpan Bek, and Mehmet Emre Tasgin, “Silent enhancement of sers signal without increasing hot spot intensities,” *Nanophotonics* **7**, 1687–1695 (2018).
- [39] Reshmi Thomas, Anoop Thomas, Saranya Pullanchery, Linta Joseph, Sanoop Mambully Somasundaran, Rotti Srinivasamurthy Swathi, Stephen K Gray, and K George Thomas, “Plexcitons: the role of oscillator strengths and spectral widths in determining strong coupling,” *ACS nano* **12**, 402–415 (2018).
- [40] MD Leistikow, Jeppe Johansen, AJ Kettelarij, Peter Lodahl, and Willem L Vos, “Size-dependent oscillator strength and quantum efficiency of cdse quantum dots controlled via the local density of states,” *Physical Review B* **79**, 045301 (2009).
- [41] Marlan O Scully and M Suhail Zubairy, “Quantum optics, Cambridge Univ. Press,” (1997).
- [42] CJ Gan and Hang Zheng, “Dynamics of a two-level system coupled to a quantum oscillator: transformed rotating-wave approximation,” *The European Physical Journal D* **59**, 473–478 (2010).
- [43] Malin Premaratne and Mark I Stockman, *Adv. Opt. Photon.*, Vol. 9 (2017) pp. 79–128.
- [44] Parinda Vasa and Christoph Lienau, “Strong light–matter interaction in quantum emitter/metal hybrid nanostructures,” *Acs Photonics* **5**, 2–23 (2017).
- [45] P Törmä and William L Barnes, “Strong coupling between surface plasmon polaritons and emitters: a review,” *Reports on Progress in Physics* **78**, 013901 (2014).